EARTHQUAKE ENGINEERING AND STRUCTURAL DYNAMICS
Earthquake Engng Struct. Dyn. 2012; **41**:177–196
Published online 8 April 2011 in Wiley Online Library (wileyonlinelibrary.com). DOI: 10.1002/eqe.1124

Analysis of the rocking response of rigid blocks standing free on a seismically isolated base

Michalis F. Vassiliou and Nicos Makris*, †, ‡

Department of Civil Engineering, University of Patras, Patras GR26500, Greece

SUMMARY

This paper examines the rocking response and stability of rigid blocks standing free on an isolated base supported: (a) on linear viscoelastic bearings, (b) on single concave and (c) on double concave spherical sliding bearings. The investigation concludes that seismic isolation is beneficial to improve the stability only of small blocks. This happens because while seismic isolation increase the 'static' value of the minimum overturning acceleration, this value remains nearly constant as we move to larger blocks or higher frequency pulses; therefore, seismic isolation removes appreciably from the dynamics of rocking blocks the beneficial property of increasing stability as their size increases or as the excitation pulse period decreases. This remarkable result suggests that free- standing ancient classical columns exhibit superior stability as they are built (standing free on a rigid foundation) rather than if they were seismically isolated even with isolation system with long isolation periods. The study further confirms this finding by examining the seismic response of the columns from the peristyle of two ancient Greek temples when subjected to historic records. Copyright © 2011 John Wiley & Sons, Ltd.

Received 28 September 2010; Revised 21 February 2011; Accepted 22 February 2011

KEY WORDS: rocking; overturning stability of slender columns; seismic isolation; spherical sliding bearings; earthquake engineering

INTRODUCTION

Under base shaking slender objects and tall rigid structures may enter into rocking motion that occasionally results in overturning. Early studies on the rocking response of a rigid block supported on a base undergoing horizontal accelerated motion were presented by Housner [1]. His pioneering work uncovered a size-frequency scale effect which explained why: (a) the larger of two geometrically similar blocks can survive the excitation that will topple the smaller block; and (b) out of two same acceleration-amplitude pulses the one with the longer duration is more capable to induce overturning.

As the size of the block increases, the duration of the coherent pulse of the base motion plays a dominant role in inducing overturning. For instance, Figure 1, plots the rocking response of a rigid block that is 2.0 m tall and 0.5 m wide when subjected to an intense ($a_p = 0.5\,g$) but short duration ($T_p = 0.5$ s) one-sine acceleration pulse (left—no overturning) and a less intense ($a_p = 0.29\,g$), yet longer duration pulse ($T_p = 2$ s) one sine acceleration pulse (right—overturning). Interestingly, this $2.0\,\text{m} \times 0.5\,\text{m}$ rigid block survives the intense, short-duration pulse; yet overturns when subjected to the lower acceleration amplitude, long-duration pulse. The above example shows that reducing

*Correspondence to: Nicos Makris, Department of Civil Engineering, University of Patras, Patras GR26500, Greece.
†E-mail: nmakris@upatras.gr
‡Professor.

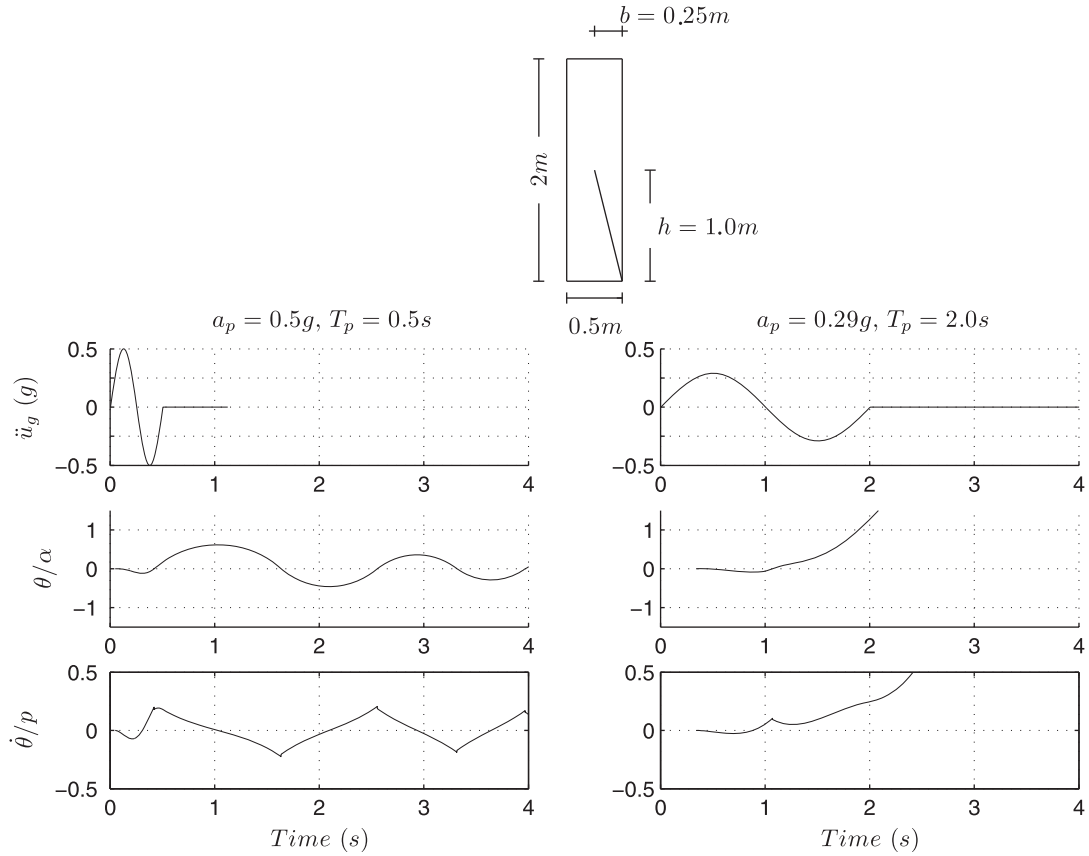

Figure 1. Horizontal ground acceleration, block rotation and angular velocity time histories of the block shown above ($p = 2.67$ rad/s, $\tan(\alpha) = 0.25$) subjected to a one-sine pulse. Left: $a_p = 0.50g$, $T_p = 0.5$ s – no overturning, Right $a_p = 0.29g < 0.5g$ and $T_p = 2.0\,\text{s} > 0.5\,\text{s}$—overturning.

the base acceleration while lengthening the period of the excitation (what seismic isolation does) may be detrimental for some combinations of block size and frequency content of the base excitation.

The rocking response of slender rigid objects standing free on a seismically isolated base is a subject that has received attention during the last two decades mainly from the need to protect slender art objects within museums ([2–6], among others). These studies primarily focused on the seismic protection of relative small size blocks such as art objects up to human-size statues and they invariably concluded that seismic isolation suppresses the rocking response and protects such objects from overturning. Given, however, the results of Figure 1, this paper investigates in depth up to what size of free-standing objects the application of seismic isolation is beneficial and concludes that larger free-standing structures like ancient columns of temples have superior stability as they stand free atop their massive foundations compared to if they were seismic isolated. Furthermore, this study settles the matter of conservation of linear momentum of the entire system (the rocking—translating block and the translating isolated base) during the impact of the rocking block—a matter that has been overlooked by other investigators.

REVIEW OF THE ROCKING RESPONSE OF A RIGID BLOCK

With reference to Figure 2 and assuming that the coefficient of friction is large enough so that there is no sliding, the equation of motion of a rocking block with size $R = \sqrt{h^2 + b^2}$ and slenderness

DOI: 10.1002/eqe

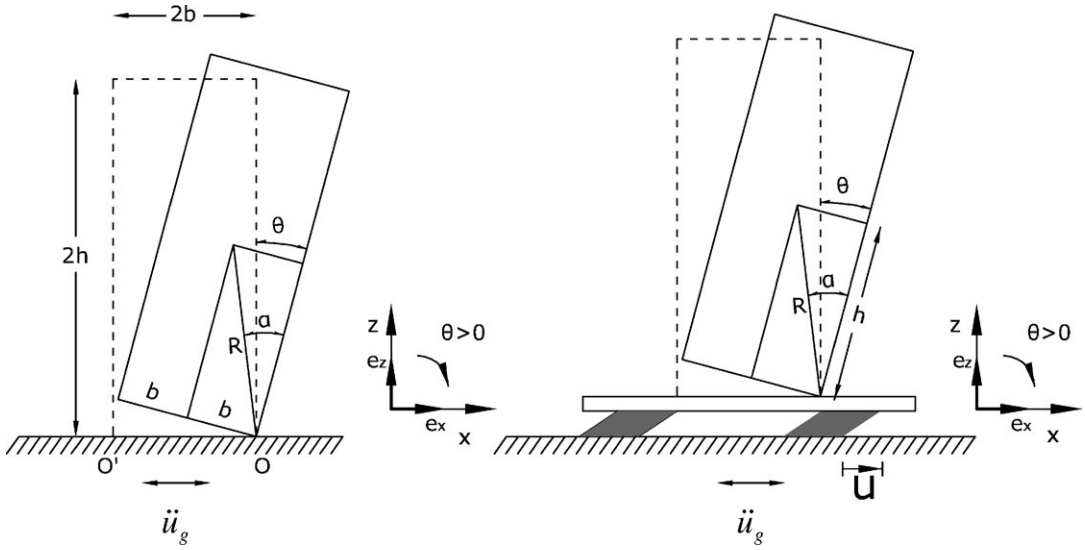

Figure 2. Geometric characteristics of the model considered. Left: Rigid block subjected to ground shaking. Right: Rigid block on isolated base.

$\alpha = a\tan(b/h)$ for rotation around O and O′ respectively is ([7–9], among others)

$$I_o\ddot{\theta}(t)+mgR\sin[-\alpha-\theta(t)] = -m\ddot{u}_g(t)R\cos[-\alpha-\theta(t)], \quad \theta(t)<0, \tag{1}$$

$$I_o\ddot{\theta}(t)+mgR\sin[\alpha-\theta(t)] = -m\ddot{u}_g(t)R\cos[\alpha-\theta(t)], \quad \theta(t)>0. \tag{2}$$

For rectangular blocks, $I_o = (4/3)mR^2$, and the above equations can be expressed in the compact form

$$\ddot{\theta}(t) = -p^2\left\{\sin[\alpha\,\mathrm{sgn}(\theta(t))-\theta(t)]+\frac{\ddot{u}_g}{g}\cos[\alpha\,\mathrm{sgn}(\theta(t))-\theta(t)]\right\}. \tag{3}$$

The oscillation frequency of a rigid block under free vibration is not constant, because it strongly depends on the vibration amplitude [1]. Nevertheless, the quantity $p=\sqrt{3g/4R}$ is a measure of the dynamic characteristics of the block. For the $2.0\,\mathrm{m}\times 0.5\,\mathrm{m}$ block shown in Figure 1 (say a modern refrigerator), $p = 2.67\,\mathrm{rad/s}$, and for a household brick, $p\approx 8\,\mathrm{rad/s}$. When the angle of rotation reverses, it is assumed that the rotation continues smoothly from points O to O′ and that the impact force is concentrated at the new pivot point, O′. The ratio of kinetic energy after and before the impact is $r=\dot{\theta}_2^2/\dot{\theta}_1^2$. Conservation of angular momentum about any pivot point just before the impact and right after the impact requires that, the maximum value of r under which a block with slenderness α will undergo rocking motion is [1]

$$r = [1-\tfrac{3}{2}\sin^2\alpha]^2. \tag{4}$$

Consequently, in order to observe rocking motion, the impact has to be inelastic.

TIME SCALE AND LENGTH SCALE OF PULSE-LIKE GROUND MOTIONS

The relative simple form, yet destructive potential of near source ground motions has motivated the development of various closed-form expressions which approximate their leading kinematic characteristics. The early work of Veletsos *et al.* [10] was followed by the papers of Hall *et al.* [11], Makris [12], Makris and Chang [13], Alavi and Krawinkler [14] and more recently by the paper of Mavroeidis and Papageorgiou [15]. Some of the proposed pulses are physically realizable motions with zero final ground velocity and finite accelerations, whereas some other idealizations

DOI: 10.1002/eqe

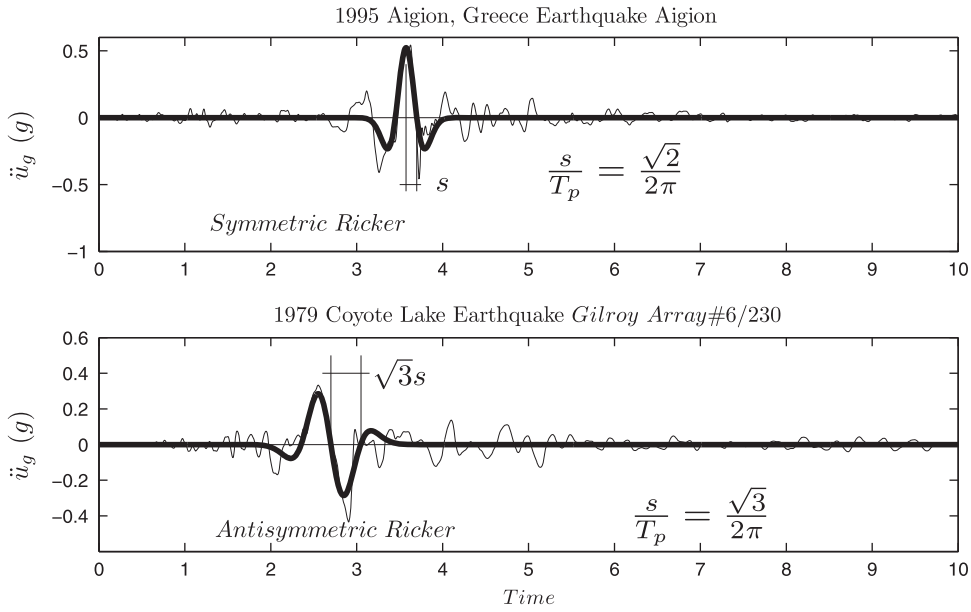

Figure 3. Acceleration time histories recorded during the: (Top) 1995 OTE FP record from the Aigion, Greece earthquake together with a symmetric Ricker wavelet; (Bottom) 1979 Coyote Lake earthquake—Gilroy Array#6/230 record together with an antisymmetric Ricker wavelet.

violate one or both of the above requirements. Physically realizable pulses can adequately describe the impulsive character of near-fault ground motions both qualitatively and quantitatively. The input parameters of the model have an unambiguous physical meaning. The minimum number of parameters is two, which are either the acceleration amplitude, a_{p}, and duration, T_{p}, or the velocity amplitude, v_{p}, and duration, T_{p} [12, 13]. The more sophisticated model of Mavroeidis and Papageorgiou [15] involves four parameters, which are the pulse period, the pulse amplitude as well as the number and phase of half cycles, and was found to describe a large set of velocity pulses generated due to forward directivity or permanent translation effect.

The heavy line in Figure 3 (top) which approximates the long-period acceleration pulse of the OTE FP record of the 1995 Aigion, Greece earthquake is a scaled expression of the second derivative of the Gaussian distribution, $\mathrm{e}^{-\frac{t^2}{2}}$, known in the seismology literature as the symmetric Ricker wavelet [16, 17] and widely referred as the 'Mexican Hat' wavelet, [18]

$$\ddot{u}_g(t) = a_{\mathrm{p}}\left(1-\frac{2\pi^2 t^2}{T_{\mathrm{p}}^2}\right)\mathrm{e}^{-\frac{1}{2}\frac{2\pi^2 t^2}{T_{\mathrm{p}}^2}} \tag{5}$$

The value of $T_{\mathrm{p}} = 2\pi/\omega_{\mathrm{p}}$ is the period that maximizes the Fourier spectrum of the symmetric Ricker wavelet.

Similarly, the heavy line in Figure 3 (bottom) which approximates the long-period acceleration pulse of the Gilroy Array #6/230 motion recorded during the 1979 Coyote Lake, earthquake is a scaled expression of the third derivative of the Gaussian distribution $\mathrm{e}^{-\frac{t^2}{2}}$. Again, in Equation (5) the value of $T_{\mathrm{p}} = 2\pi/\omega_{\mathrm{p}}$ is the period that maximizes the Fourier spectrum of the antisymmetric Ricker wavelet.

$$\ddot{u}_g(t) = \frac{a_{\mathrm{p}}}{\beta}\left(\frac{4\pi^2 t^2}{3T_{\mathrm{p}}^2}-3\right)\frac{2\pi t}{\sqrt{3}T_{\mathrm{p}}}\mathrm{e}^{-\frac{1}{2}\frac{4\pi^2 t^2}{3T_{\mathrm{p}}^2}} \tag{6}$$

in which β is a factor equal to 1.38 that enforces the above function to have a maximum = a_{p}. Ricker wavelets have been popular in studying the effects of near-fault ground motions [19, 20] among others.

DOI: 10.1002/eqe

The choice of the specific functional expression to approximate the main pulse of pulse-type ground motions has limited significance in this work. In the past simple trigonometric pulses have been used by the senior author [13, 14, 20, 21] to extract the time scale and length scale of pulse-type ground motions.

A mathematically rigorous and easily reproducible methodology based on wavelet analysis to construct the best matching wavelet on a given record (signal) has been recently proposed by Vassiliou and Makris [22].

ROCKING RESPONSE OF A RIGID BLOCK STANDING FREE ON A SEISMICALLY ISOLATED BASE

Linear viscoelastic isolation system

We consider a rigid block with mass, m, slenderness α, and frequency parameter p, standing free on a seismically isolated base with mass m_b, horizontal linear stiffness k_b and viscous damping c_b, as shown in Figure 2 (right). The equation of motion can be derived from Equation (3) by substituting $\ddot{u}_g$ with $\ddot{u}_g+\ddot{u}$, where u is the displacement of the isolated base relative to the ground. Then, Equation (3) becomes

$$\ddot{\theta}(t)=-p^2\left\{\sin[\alpha\mathrm{sgn}(\theta(t))-\theta(t)]+\frac{\ddot{u}_g(t)+\ddot{u}(t)}{g}\cos[\alpha\mathrm{sgn}(\theta(t))-\theta(t)]\right\}. \tag{7}$$

Moreover, horizontal force equilibrium of the isolated base below isolators gives

$$-k_\mathrm{b}u-c_\mathrm{b}\dot{u}=m_\mathrm{b}(\ddot{u}_g+\ddot{u})+m(\ddot{u}_g+\ddot{u}+\ddot{x}), \tag{8}$$

where x is the horizontal, relative to the base translation of the center of mass of the rigid block given by

$$x(t)=\mathrm{sgn}(\theta(t))R\sin(a)-R\sin(\mathrm{sgn}(\theta(t))\alpha-\theta(t)). \tag{9}$$

Equations (7) and (8) are expressed in terms of $\ddot{u}$ and $\ddot{\theta}$ which are explicit expressions of the four states of the system, $u(t)$, $\dot{u}(t)$, $\theta(t)$, $\dot{\theta}(t)$ in order to solve the system of equations explicitly. Accordingly,

$$\ddot{u}(t)=\frac{-\omega_\mathrm{b}^2u(t)-2\xi\omega_n\dot{u}(t)-\gamma R(\dot{\theta}(t))^2\sin A(t)+\gamma Rp^2\cos A(t)\sin A(t)}{1-\dfrac{\gamma Rp^2\cos^2 A(t)}{g}}-\ddot{u}_g(t), \tag{10}$$

$$\ddot{\theta}(t)=-p^2\left(\sin A(t)+\cos A(t)\left(\frac{-\omega_n^2u(t)-2\xi\omega_n\dot{u}(t)-\gamma R(\dot{\theta}(t))^2\sin A(t)+\gamma Rp^2\cos A(t)\sin A(t)}{g-\gamma Rp^2\cos^2 A(t)}\right)\right), \tag{11}$$

where the term $A(t)=\alpha\mathrm{sgn}\theta(t)-\theta(t)$ and $\gamma=m/(m_\mathrm{b}+m)$ and $\omega_\mathrm{b}=\sqrt{k_\mathrm{b}/(m_\mathrm{b}+m)}$.

Again, in this case we assume that when the angle of rotation reverses, the rotation of the block continues smoothly from point O to O′ and that the impact force is concentrated as a point force which applies on the new pivot point O′. The subtle difference between a rocking block impacting a base with finite mass, m_b, and a rocking block impacting a rigid foundation with infinite mass, is that the translational velocity of the isolated base also experiences a finite jump during impact, whereas the translational velocity of the rigid foundation with infinite mass remains the same during impact.

With reference to Figure 4, conservation of angular momentum around point O′ gives

$$\int_{\mathrm{block}}\mathbf{r}\times(\dot{\mathbf{v}}_1+\dot{\mathbf{u}}_1)\,\mathrm{d}m=\int_{\mathrm{block}}\mathbf{r}\times(\dot{\mathbf{v}}_2+\dot{\mathbf{u}}_2)\,\mathrm{d}m \tag{12}$$

DOI: 10.1002/eqe

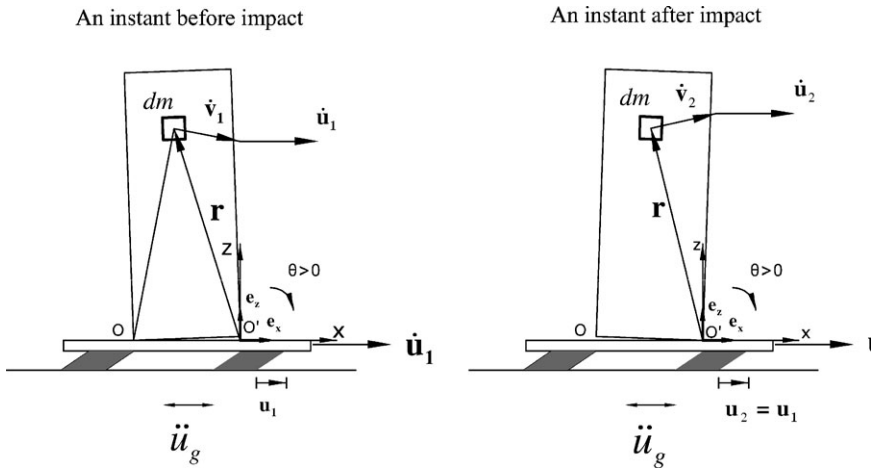

Figure 4. Rigid block rocking on an isolated base before (left) and after (right) the impact.

where $\dot{\mathbf{v}}_1$ and $\dot{\mathbf{v}}_2$ are the velocities (with respect to the isolated base) of a point mass due to rotation before and after the impact and $\dot{\mathbf{u}}_1$ and $\dot{\mathbf{u}}_2$ are the translational velocities of the base (with respect to the ground) before and after the impact. Equation (12) gives

$$(I_o\dot{\theta}_1 - 2mRb\sin\alpha\dot{\theta}_1)\mathbf{e}_y + \int_{\text{block}} \mathbf{r}\times\dot{\mathbf{u}}_1\,\dot{m} = I_o\dot{\theta}_2\mathbf{e}_y + \int_{\text{block}} \mathbf{r}\times\dot{\mathbf{u}}_2\,dm \tag{13}$$

or

$$I_o\dot{\theta}_1 - 2mRb\sin\alpha\dot{\theta}_1 + mh\dot{u}_1 = I_o\dot{\theta}_2 + mh\dot{u}_2. \tag{14}$$

For a rectangular block $I_o = \frac{4}{3}mR^2$ and the above expression reduces to

$$4R^2\dot{\theta}_1 - 6Rb\sin\alpha\dot{\theta}_1 + 3h\dot{u}_1 = 4R^2\dot{\theta}_2 + 3h\dot{u}_2 \tag{15}$$

Equation (15) indicates that because of the finite mass of the isolation base one has to determine the translational velocity of the base $\dot{u}_2$ after the impact. The extra equation that is needed to relate $\dot{u}_1$ and $\dot{u}_2$ is the conservation of the linear momentum of the entire system (the rocking—translating block together with the translating base) along the horizontal direction. Accordingly

$$(m+m_b)\dot{u}_1 + mh\dot{\theta}_1 = (m+m_b)\dot{u}_2 + mh\dot{\theta}_2 \tag{16}$$

or

$$(\gamma+1)\dot{u}_1 + \gamma h\dot{\theta}_1 = (\gamma+1)\dot{u}_2 + \gamma h\dot{\theta}_2 \tag{17}$$

From Equations (15) and (17) one obtains

$$\dot{\theta}_2 = \frac{(\gamma+4)\cot^2\alpha - 2(\gamma+1)}{(\gamma+4)\cot^2\alpha + 4(\gamma+1)}\dot{\theta}_1 \tag{18}$$

and

$$\dot{u}_2 = \dot{u}_1 + \frac{6\gamma h}{(\gamma+4)\cot^2\alpha + 4(\gamma+1)}\dot{\theta}_1. \tag{19}$$

Note that in the limiting case of a very heavy base ($m_b \to \infty$ or $\gamma \to 0$) Equation (18) reduces to Equation (4); while $\dot{u}_1 = \dot{u}_2$; therefore the situation of a block rocking on a rigid foundation

DOI: 10.1002/eqe

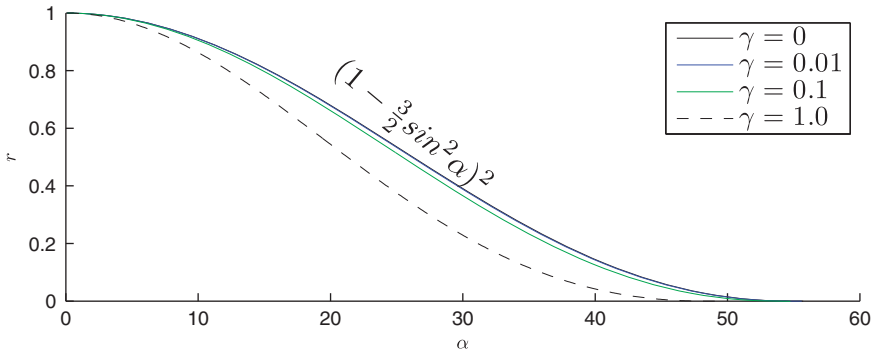

Figure 5. Maximum values of the coefficient of restitution, r, for different values of $\gamma = m/(m+m_b)$ under which an isolated block with slenderness α can undergo rocking motion.

is recovered. From Equation (18) the maximum value of the coefficient of restitution that allows rocking motion of a block rocking on an isolated base is

$$r = \left(\frac{\dot{\theta}_2}{\dot{\theta}_1}\right)^2 = \left(\frac{(\gamma+4)\cot^2\alpha - 2(\gamma+1)}{(\gamma+4)\cot^2\alpha + 4(\gamma+1)}\right)^2. \tag{20}$$

The expression of the coefficient of restitution given by (20) is in agreement with an equivalent expression presented by Roussis *et al.* [5], which, to our knowledge is the only past publication that treats this problem correctly.

Figure 5 plots the expression given by Equation (20) for three values of $\gamma = m/m + m_b = 0.01$, 0.1 and 1. Figure 5 indicates that when the mass of the base is finite, the rocking block needs to loose additional energy during impact in order to undergo rocking motion (compared with the same block rocking on a rigid foundation) due to the reason that the translational velocity of the isolated base experiences a finite jump at the instant of the impact.

Overturning spectra—self-similar response

We consider again that the ground excitation of the system shown in Figure 2 is characterized by a coherent acceleration pulse with amplitude a_p and pulse duration $T_p = 2\pi/\omega_p$. From Equations (10) and (11) it results that the response of a rocking block standing free on an isolated base subjected to an acceleration pulse is a function of eight (8) variables

$$u(t) = f(p, \alpha, g, \omega_b, \xi, \gamma, \alpha_p, \omega_p), \tag{21}$$

$$\theta(t) = f(p, \alpha, g, \omega_b, \xi, \gamma, \alpha_p, \omega_p). \tag{22}$$

Each of the coupled Equations (10) and (11) $\theta \doteq [\cdot]$, $u_\cdot \doteq [L]$, $a_{p\cdot} \doteq [L][T]^{-2}$, $T_p \doteq [T]$, $T_b \doteq [T]$, $\xi \doteq [\cdot]$, $p_\cdot \doteq [T]^{-1}$, $\alpha \cdot \doteq []$, $g \cdot \doteq [L][T]^{-2}$, $\gamma \doteq []$ involves only two reference dimensions; that of length $[L]$ and time $[T]$. According to Buckingham's Π-theorem the number of dimensionless products (Π-Terms)=(number of variables in Equation (10) and (11)=10)–(number of reference dimensions=2); therefore for the two DOF systems described above, there are $10-2=8\Pi$–terms

$$\Pi_m = \frac{u_{\max}\omega_p^2}{a_p}, \tag{23}$$

$$\Pi_\theta = \theta, \tag{24}$$

$$\Pi_\omega = \frac{\omega_b}{\omega_p}, \tag{25}$$

$$\Pi_\xi = \xi, \tag{26}$$

DOI: 10.1002/eqe

$$\Pi_\gamma = \gamma, \tag{27}$$

$$\Pi_{\mathrm{p}} = \frac{\omega_{\mathrm{p}}}{p}, \tag{28}$$

$$\Pi_a = \tan(\alpha), \tag{29}$$

$$\Pi_g = \frac{a_{\mathrm{p}}}{g}. \tag{30}$$

The rocking response of a rigid block standing free on an isolated base subjected to a horizontal base acceleration is computed by solving Equations (10) and (11) in association with the minimum energy loss expression given by Equation (20) which takes place at every impact. In this case, the state vector of the system shown in Figure 2 (right) for linear viscoelastic bearings is

$$\mathbf{y}(t) = \begin{bmatrix} u(t) \\ \dot{u}(t) \\ \theta(t) \\ \dot{\theta}(t) \end{bmatrix} \tag{31}$$

and the time derivative vector $\mathbf{f}(t) = \dot{\mathbf{y}}(t)$ is

$$\dot{\mathbf{y}}(t) = \begin{bmatrix} \dot{u}(t) \\ \dfrac{-\omega_{\mathrm{b}}^2 u(t) - 2\xi\omega b\dot{u}(t) - \gamma R(\dot{\theta}(t))^2 \sin A(t) + \gamma R \cos A(t) p^2 \sin A(t)}{1 - \frac{\gamma R p^2 \cos^2 A(t)}{g}} - \ddot{u}_g(t) \\ \ddot{\theta}(t) \\ -p^2 \left(\sin A(t) + \cos A(t) \left(\dfrac{-\omega_{\mathrm{b}}^2 u(t) - 2\xi\omega b\dot{u}(t) - \gamma R(\dot{\theta}(t))^2 \sin A(t) + \gamma R \cos A(t) p^2 \sin A(t)}{g - \gamma R p^2 \cos A(t)} \right) \right) \end{bmatrix}. \tag{32}$$

The numerical integration of (17) is performed with standard Ordinary Differential Equations (ODE) solvers available in MATLAB [23].

Figure 6 plots the overturning acceleration spectra for a rigid block with slenderness $\alpha = 10^\circ$ (top) and $\alpha = 20^\circ$ (bottom) when it is standing free on a rigid foundation (left), and when it is isolated (center and right) and subjected to a symmetric Ricker wavelet. The viscous damping ratio of the bearings is $\xi = 5\%$ and the mass ratio is $\gamma = 0.01$ (heavy base). Figure 6 indicates that the presence of the isolation base increases the 'static' overturning acceleration; however, for isolated rigid blocks this 'static' value remains nearly constant as the ratio ω_{p}/p increases (moving to larger blocks or high-frequency pulses). Consequently, the presence of an isolation base removes appreciably from the dynamics of rocking blocks the fundamental property of increasing stability as their size increases or as the excitation pulse-period decreases. Nevertheless, the finding that seismic isolation increases the value of the uplift acceleration of slender free-standing objects has practical significance when protecting delicate artifacts in which any kind of damage due to impact shall be avoided.

The findings of Figure 6 together with results due to an antisymmetric Ricker excitation are summarized in Figure 7 in terms of minimum acceleration overturning spectra. In all configurations beyond a certain value of ω_{p}/p the minimum overturning acceleration spectrum of the free-standing block on a rigid base (heavy dark line) crosses the overturning acceleration spectrum of the same block when isolated. Accordingly there is no point in isolating large free-standing blocks. Note also that for both symmetric (left plots) and antisymmetric (right plots) Ricker wavelets, the minimum overturning acceleration of the free-standing block on a rigid foundation exceeds the overturning acceleration of the isolated configuration at smaller values of ω_{p}/p as the slenderness of the block decreases (larger values of α).

DOI: 10.1002/eqe

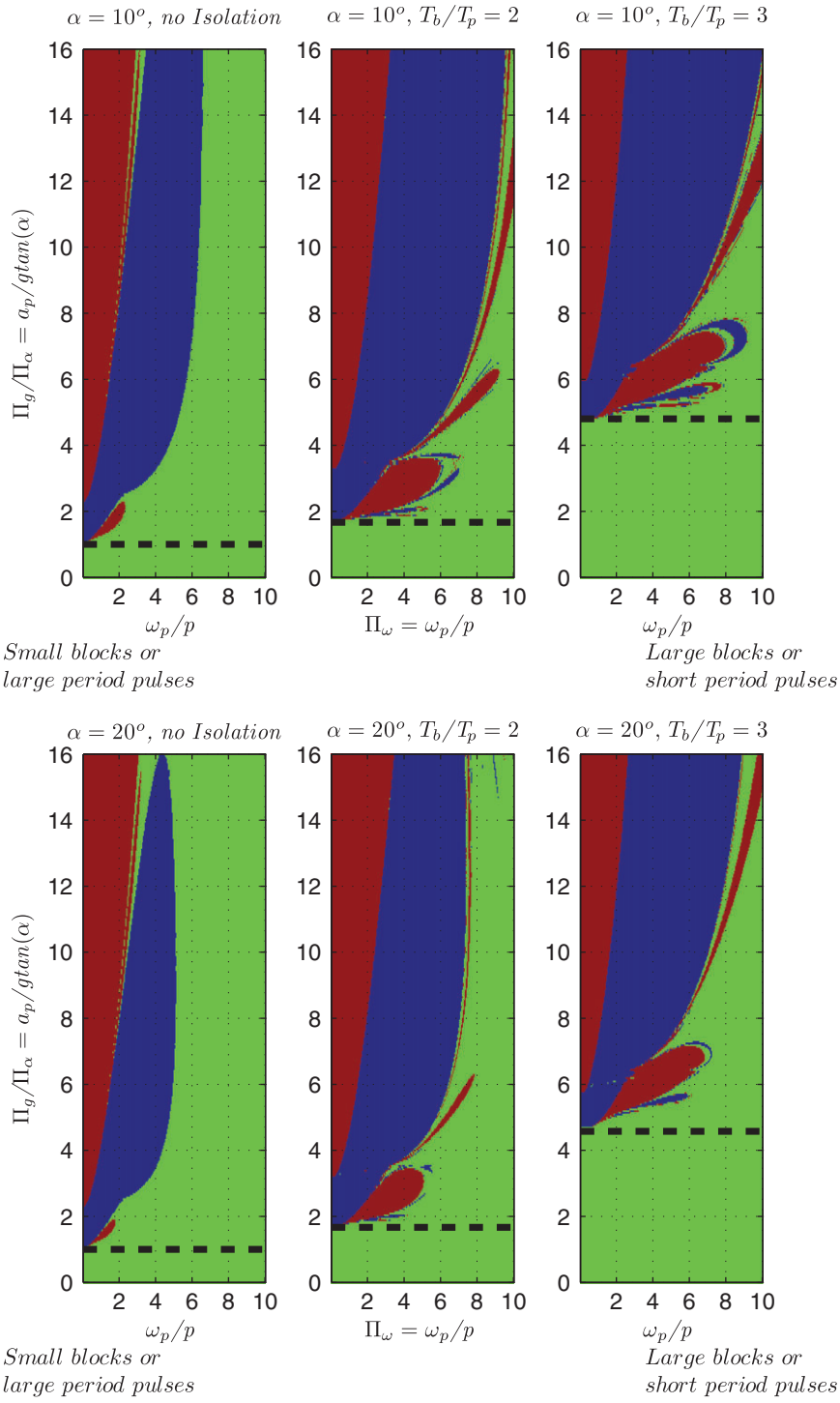

Figure 6. Overturning spectra for rigid block without isolation (left), and with linear isolation with $T_b/T_p = 2$ (center) and $T_b/T_p = 3$ for slenderness $\alpha = 10^\circ$ (top) and $\alpha = 20^\circ$ (bottom) for a symmetric Ricker excitation. Light gray = no overturning, dark gray = overturning.

The practical use of the results shown in Figure 7 is illustrated by considering the dominant pulses that capture the coherent component of the two out of the three earthquake records shown in Figure 3—that of the fault parallel component of the OTE record from the 1995 Aigio, Greece

DOI: 10.1002/eqe

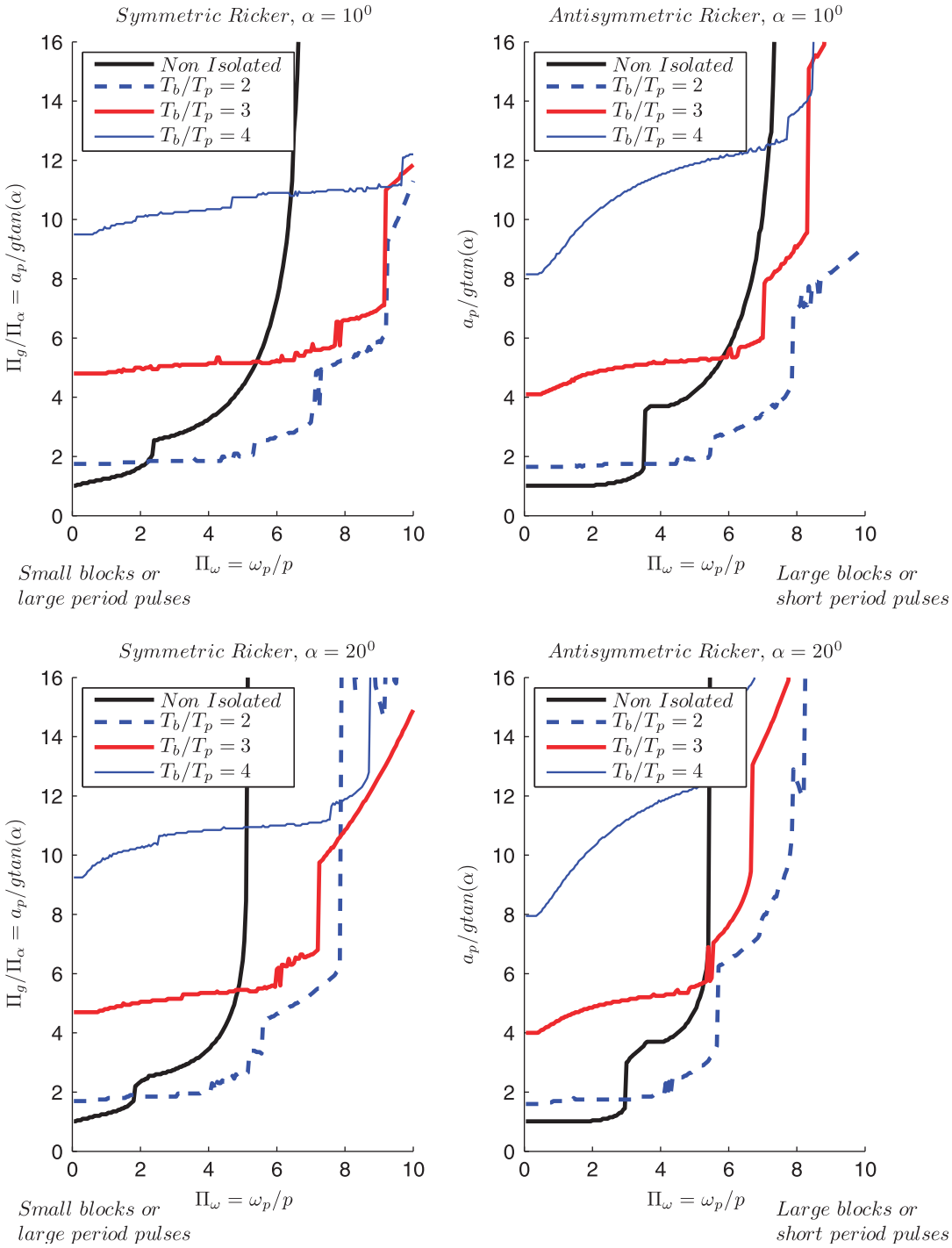

Figure 7. Comparison of the minimum acceleration needed to overturn a rigid block of slenderness $\alpha = 10^\circ$ ($h/b = 5.67$–top) and $\alpha = 20^\circ$ ($h/b = 2.75$–bottom) resting on rigid ground and on an isolated bases with various isolation frequencies when excited by a symmetric Ricker pulse (left) or an antisymmetric Ricker pulse (right).

earthquake (top), that of the Gilroy—Array #6 record from the 1979 Coyote Lake , USA earthquake (center). For the FP OTE record shown in Figure 3 (top), $T_p = 0.6$ s while for the Coyote Lake record (bottom), $T_p = 0.9$ s. The corresponding values of the semidiagonal, R, beyond which

DOI: 10.1002/eqe

non-isolated free-standing blocks exhibit more stability than when seismic isolated are offered in Table I for two values of slenderness $\alpha=10^\circ$ and $\alpha=20^\circ$ and three values of T_b/T_p 2, 3 and 4. Table I applies the information offered in Figure 7 to typical values of seismic isolation periods and pulse periods from the two strong, pulse-like ground motions which are compatible with the seismic hazard in Greece. Note that for the OTE record from the 1995 Aigio, Greece earthquake ($T_p=0.6$ s) free-standing objects even smaller than ancient classical columns ($R\approx 3.5$–5.0 m) are more stable when they stand free on a rigid foundation rather than when they rest on a seismically isolated base. For the Gilroy#6 record of the Coyote Lake earthquake ($T_p=0.9$ s) seismic isolation becomes beneficial when the isolation period is in the long-period range ($T_b>2.5$ s).

The influence of the mass ratio $\gamma=m/(m+m_b)$ ($m=$mass of the rocking block, $m_b=$mass of the isolated base) is shown in Figure 8 for a block with slenderness $\alpha=12^\circ$, two values of

Table I. Length of the semidiagonal, R, of rigid blocks beyond which they exhibit superior stability when they stand free on a rigid base (no isolation).

		$T_b/T_p=2$			$T_b/T_p=3$			$T_b/T_p=4$		
			$R_{critical}$ (m)			$R_{critical}$ (m)			$R_{critical}$ (m)	
	T_p (s)	T_b (s)	10°	20°	T_b (s)	10°	20°	T_b (s)	10°	20°
Aigio, OTE FP, 1995	0.6	1.2	0.32	0.22	1.8	1.96	1.58	2.4	2.79	1.78
Coyote Lake, Gilroy #6 230, 1979	0.9	1.8	1.85	1.31	2.7	5.08	4.24	3.6	7.83	4.48

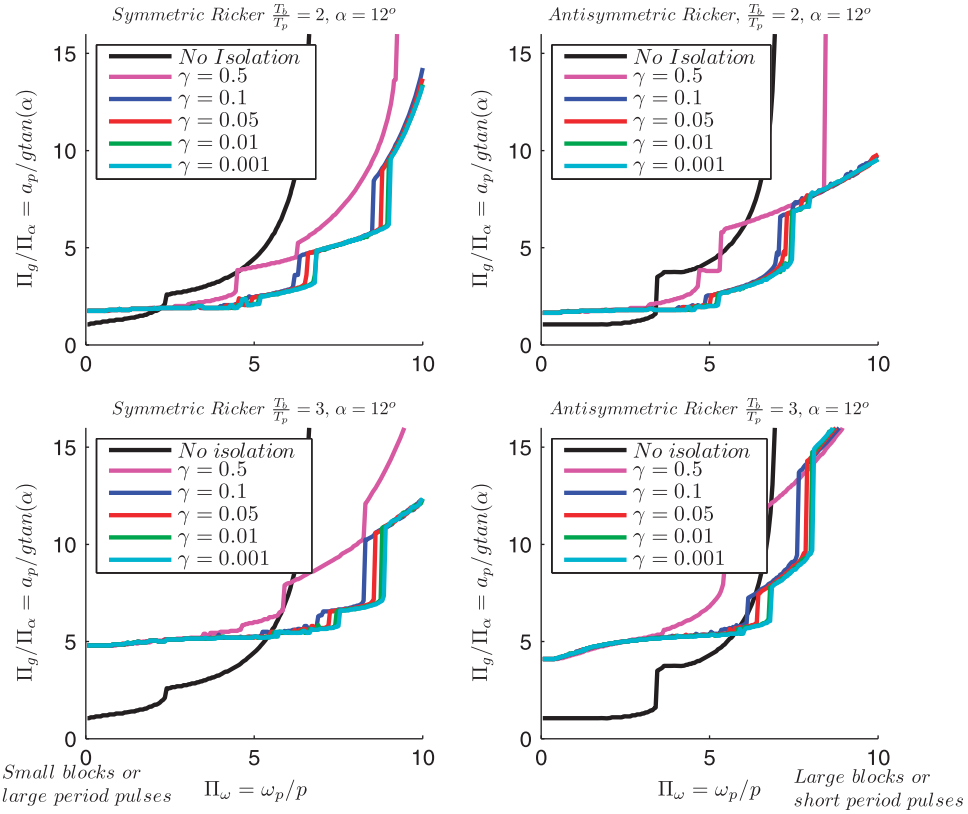

Figure 8. Comparison of the minimum acceleration needed to overturn a rigid block of slenderness $\alpha=12^\circ$ ($h/b=4.70$) resting on a linear viscoelastic isolated base subjected to a symmetric Ricker wavelet (left) and an antisymmetric Ricker wavelet (right). The results for five values of mass ratio $\gamma=m/(m+m_b)$ are used showing that for values of $\gamma<0.1$ the overturning acceleration does not depend on the mass ratio $\gamma=m/(m+m_b)$.

DOI: 10.1002/eqe

$T_b/T_p=2$ and three and five values of γ. Figure 8 indicates that for values of $\omega_p/p<6$ (the range when it makes sense to isolate rocking blocks) all response curves for $\gamma\leqslant 0.1$ tend to the finite limit where the response of the heavy base is not influenced by the response of the light rocking block (decoupled system). Consequently for the case where $\gamma\leqslant 0.1$ the mass ration γ drops out of consideration ($\gamma=0$) and it can be eliminated from equations (32) and (33)—a conclusion that shows that the rocking response of a rigid block standing free on an isolated base exhibits a 'complete similarity' in terms of the mass ratio $\gamma=m/(m+m_b)$.

Bilinear isolation system

When the behavior of the isolation system is bilinear—a very good idealization for the behavior of spherical sliding bearings and lead rubber bearings, the equation of the rocking block is again given by Equation (7) whereas, horizontal equilibrium of the isolated base below isolators gives

$$-k_b u(t)-Q\cdot z(t)=m_b(\ddot{u}_g(t)+\ddot{u}(t))+m(\ddot{u}_g(t)+\ddot{u}(t)+\ddot{x}(t)) \tag{33}$$

where k_b is the second slope of the bilinear idealization, Q is the strength of the system (force at zero displacement), $x(t)$ is the horizontal relative to the base translation of the center of mass of the rigid block and $z(t)$ is a dimensionless parameter of the Bouc–Wen model given by

$$\dot{z}(t)=\frac{1}{u_y}(\dot{u}(t)-\gamma|\dot{u}(t)|z(t)|z(t)|^{n-1}-\beta\dot{u}(t)|z(t)|^n), \tag{34}$$

where u_y is the yield displacement of the bilinear behavior.

In this paper our study concentrates in the case where u_y is very small ($u_y\approx 0.25$ mm). In this case the bilinear model is the mathematical description of the spherical sliding bearing with coefficient of friction μ, in which case the strength $Q=\mu(m+m_b)g$. Past studies led by the senior authors [13, 24, 25] have demonstrated that the response of isolated structures is merely indifferent to the exact value of the yield displacement; therefore, the results obtained in this paper are also valid for isolation systems that use lead–rubber bearings (larger values of u_y) as long as they experience the same second slope, k_b, and the same strength, Q. Given Equations (33) and (34), together with Equation (7) the state vector of the system shown in Figure 2 (right) with spherical sliding bearings is:

$$\mathbf{y}(t)=\begin{bmatrix} u(t)\\ \dot{u}(t)\\ z(t)\\ \theta(t)\\ \dot{\theta}(t)\end{bmatrix} \tag{35}$$

$$\dot{\mathbf{y}}(t)=\begin{bmatrix} \dot{u}(t)\\ \dfrac{-\omega_b^2u(t)-\mu g z(t)-\gamma R(\dot{\theta}(t))^2\sin A(t)+\gamma R\cos A(t)p^2\sin A(t)}{1-\frac{\gamma Rp^2\cos^2 A(t)}{g}}-\ddot{u}_g(t)\\ \dfrac{1}{u_y}(\dot{u}(t)-\gamma|\dot{u}(t)|z(t)|z(t)|^{n-1}-\beta\dot{u}(t)|z(t)|^n)\\ \dot{\theta}(t)\\ -p^2\left(\sin A(t)+\cos A(t)\left(\dfrac{-\omega_b^2u(t)-\mu g z(t)-\gamma R(\dot{\theta}(t))^2\sin A(t)+\gamma R\cos A(t)p^2\sin A(t)}{g-\gamma Rp^2\cos A(t)}\right)\right)\end{bmatrix} \tag{36}$$

In the case where the base is isolated on lead rubber bearings exhibiting a strength Q, the term μg in the 2nd and 5th component of the $\dot{\mathbf{y}}(t)$ vector is replaced with $\frac{Q}{m+m_b}$.

DOI: 10.1002/eqe

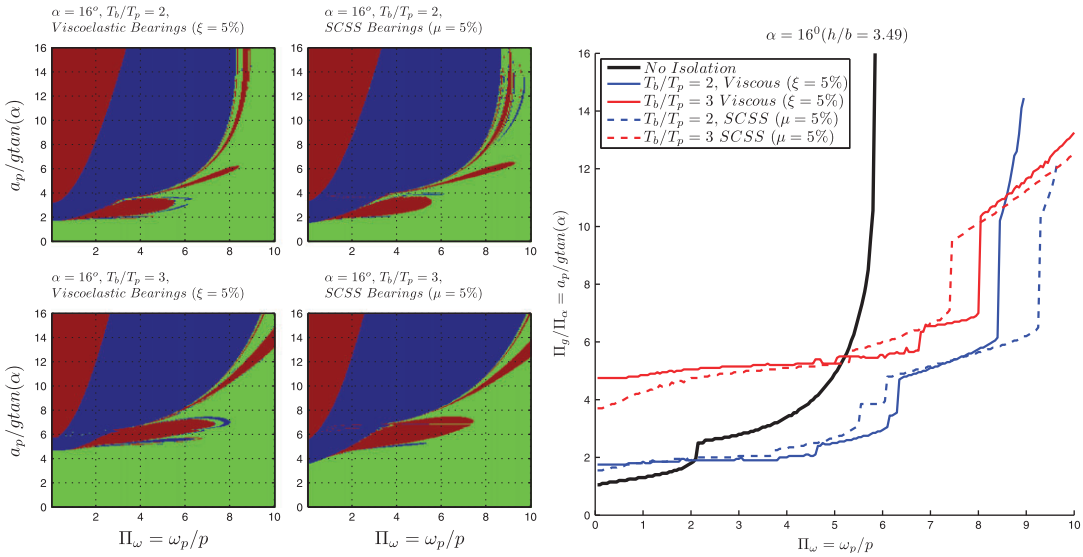

Figure 9. Comparison of overturning spectra (left) and minimum acceleration overturning spectra (right) of a rigid body with slenderness $\alpha = 16^\circ$ $(h/b = 3.49)$ when the supporting base is isolated on viscoelastic bearings with damping ratio $\xi = 5\%$ and single concave spherical sliding bearings with coefficient of friction 5%. The excitation is a symmetric Ricker wavelet and the mass ratio $\gamma = 0.01$. Light gray = no overturning, dark gray = overturning.

Figure 9 plots overturning spectra of a rigid block with slenderness $\alpha = 16^\circ$ $(h/b = 3.49)$ standing free on a base that is isolated on single concave spherical sliding bearings with coefficient of friction $\mu = 5\%$ when subjected to a symmetric Ricker wavelet next to the overturning acceleration spectra when the base is isolated on linear viscoelastic bearings with coefficient $\xi = 5\%$. The response between the two isolation configurations is very similar. For completeness, Figure 9 (bottom) shows the minimum overturning acceleration associated with the two isolation configurations together with the corresponding spectrum of a rigid block rocking on a rigid foundation (heavy dark line). The near-vertical growth of the heavy dark line indicates that regardless how flexible the isolation system is, for values of $\omega_p/p > 6$, the rigid block rocking on a rigid foundation has superior stability.

Trilinear isolation system (*Double concave spherical sliding* (*DCSS*) *bearings*)

The rapid growth of seismic isolation generated the need for more compact size, large-displacement capacity, long-period, bearings. Such needs are served with the DCSS bearing—its configuration is shown schematically in Figure 10 (left) [26–30] among others). When the double concave spherical bearing has sliding surfaces with the same coefficient of friction, μ, (no need for same radii of curvature) it becomes like a traditional single concave spherical bearing with isolation period $T_b = 2\pi\sqrt{\frac{R_1+R_2-h_1-h_2}{g}}$ and coefficient of friction μ.

When the coefficients of friction along the sliding interfaces are different, the behavior of the double concave friction spherical bearing is trilinear and it can be modeled using two traditional single concave spherical bearings acting in series together with a point mass representing the articulated slider. With this mathematically rigorous model one can capture the shaved portions of the hysteretic loops at the initiation and at the reversal of motion (see Figure 10—right) when, initially, the sliding surface with the lower coefficient of friction is mobilized.

Recently, Makris and Vassiliou [24] have shown that for most practical configurations the area of the shaded triangles shown in Figure 10 (right) is immaterial to the peak response of an isolated deck; therefore, the deck exhibits merely the same maximum displacement regardless whether it

DOI: 10.1002/eqe

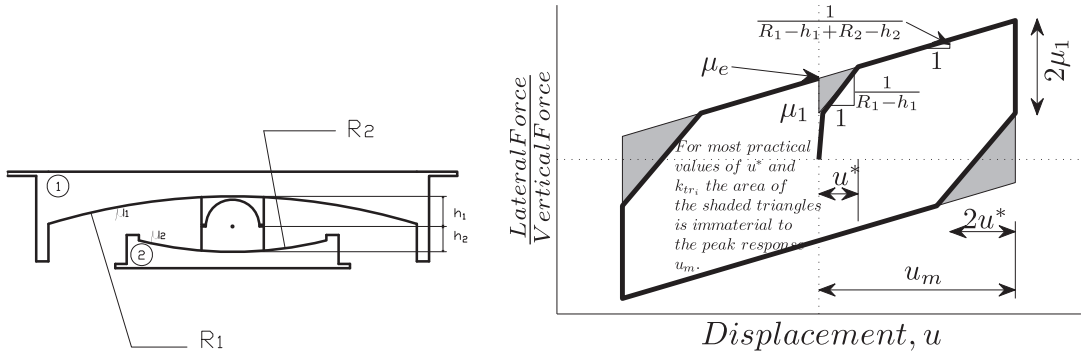

Figure 10. Left: Cross-section of a double concave spherical sliding (DCSS) bearing with different radii of curvature; Right: Generic force–displacement loop of the DCSS bearing (heavy line).

is supported on a double concave (R_1-h_1, R_2-h_2, μ_1, μ_2) or single concave (R_e, μ_e) spherical sliding bearing provided that

$$\frac{1}{R_e}=\frac{1}{R_1-h_1+R_2-h_2} \tag{37}$$

and

$$\mu_e=\frac{\mu_1(R_1-h_1)+\mu_2(R_2-h_2)}{R_1-h_1+R_2-h_2}. \tag{38}$$

The aim of this analysis is to examine whether the selection of a lower coefficient of friction in one sliding surface may increase the merit of seismic isolation to protect rocking structures. The friction coefficients of two alternative DCSS systems are selected so that their equivalent coefficient of friction given by Equation (39) is $\mu_e=5\%$. The first configuration of the DCSS system assumes bearings with the same top and bottom radius of curvatures, $R_1-h_1=R_2-h_2$. For this configuration we have assumed $\mu_1=3\%$ and $\mu_2=7\%$ in order to have appreciable separation between the two values of the friction coefficients. The second configuration of the DCSS system assumes bearings with $R_2-h_2=2(R_1-h_1)$, $\mu_1=3\%$ and now $\mu_2=6\%$ in order for μ_e to yield $\mu_e=5\%$.

Figure 11 plots minimum overturning acceleration spectra of free-standing blocks with slenderness $\alpha=16^\circ$ ($h/b=3.49$) standing free on a base isolated on DCSS bearings when $T_b/T_p=2$ and 3. The computed results when the isolation system consists of the DCSS bearings are compared with the results obtained when the isolation system consists of single concave spherical sliding (SCSS) bearings with coefficient of friction $\mu_1=\mu_e=5\%$ and is concluded that for all practical purposes that the minimum overturning acceleration for the three configurations is identical.

This finding shows that the area of the shaded triangles shown in Figure 10 (right) is indeed immaterial to the stability of the isolated rocking block. In mathematical terms, the minimum overturning acceleration of a rocking block standing free on a base isolated with bearings with trilinear behavior exhibits a complete similarity in (a) the difference between the coefficients of friction and (b) the ratio of the intermediate (transition) to the final slope. Most importantly, Figure 11 confirms what has been shown throughout this study that beyond a certain value of ω_p/p (beyond a center block size/pulse duration) the application of seismic isolation has a detrimental effect on the stability of rocking blocks since blocks standing free on a rigid foundation exhibit superior stability.

THE EFFECT OF SEISMIC ISOLATION ON ANCIENT CLASSICAL COLUMNS

The seismic response analysis of rocking blocks standing free on an isolated base has been studied in this paper by using as ground excitation, acceleration pulses described either by the symmetric

DOI: 10.1002/eqe

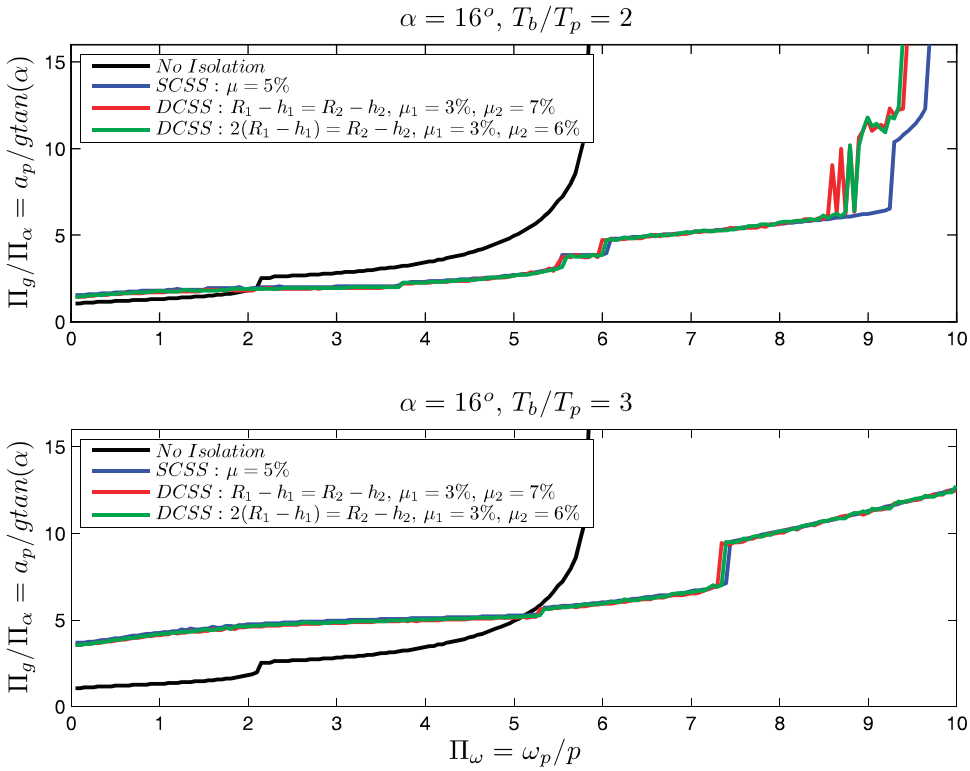

Figure 11. Comparison of minimum acceleration overturning spectra of a rigid body with slenderness $\alpha = 16^\circ$ ($h/b = 3.49$) when the supporting base is isolated on double concave and single concave spherical sliding bearings. The excitation is a symmetric Ricker wavelet and the mass ratio $\gamma = 0.01$.

or the antisymmetric Ricker wavelets. The acceleration amplitude, a_p, and duration T_p of any distinct acceleration pulse allow the use of the dimensional analysis presented in this work and the derivation of the associated Π-products which improve appreciably the understanding of the physics that governs the problem together with the organization and presentation of the response quantities in a most meaningful way. Nevertheless, in order to stress the main finding of this study—that for large blocks (say $\omega_p/p > 6$) the use of seismic isolation reduces the seismic stability of free-standing rocking structures—we examine the seismic response of two free-standing slender blocks which have the dimensions of the columns of the peristyle of the Temple of Appolo at Bassae and the Temple of Zeus at Nemea, both located in Peloponese, Greece.

The Temple of Apollo at Bassae is a fifth Century BC doric style structure. The columns of the temple are 5.95 m high, the diameter of the base drum is 1.11 m (resulting in slenderness $\alpha = 10.56^\circ$ ($h/b = 5.36$) and in size $R = 3.03$ m). The number of drums in each column is not constant for all the columns and is controlled by the size of the sound rock that was available in the ancient limestone quarry. The temple is still standing but has suffered from erosion of the building material caused by the adverse climatic conditions at the site (1000 m altitude above the sea level) and from the tilting of some columns due to differential settlement of the foundations [31].

The Temple of Zeus at Nemea was built in the late fourth century BC. The columns of this temple are much taller and more slender than the ones of the temple at Bassae, reaching a height of 10.33 m. All columns consist of 13 drums and the base drum diameter is 1.52 m. The resulting slenderness is $\alpha = 8.37^\circ$ ($h/b = 6.8$) and $R = 5.22$ m. This slenderness ratio is the smallest among the ancient Greek temples of continental Greece. Only one column of the peristyle and two columns of the pronaos of the Temple of Zeus remain standing from the ancient times.

While the columns from the two abovementioned Temples are multidrum, this investigation proceeds with the approximation that they are monolithic free standing blocks. Past studies led

DOI: 10.1002/eqe

Table II. Earthquake records used for the dynamic response analysis of the column.

Earthquake	Record station	Magnitude (Mw)	Distance (km)	PGA (g)	PGV (m/s)	a_p (g)	T_p (s)
1966 Parkfield	CO2/065	6.1	0.1	0.48	0.75	0.41	0.6
1977 Vrancea	Bucharest	7.2	160	0.20	0.74	0.20	2.1
1979 Imperial Valley	El Centro #6/230	6.5	9.3	0.41	0.65	0.14	3.1
1980 Irpinia, Italy	Sturno/270	6.5	32	0.36	0.52	0.11	3.0
1986 San Salvador	Geotech Investig. Center	5.4	4.3	0.48	0.48	0.34	0.8
1987 Superstition Hills	Parachute Test Site/225	6.7	0.7	0.45	1.12	0.30	2.0
1992 Erzican,	Erzincan/EW	6.9	13	0.50	0.64	0.34	0.9
1994 Northridge	Jensen Filter Plant/022	6.7	6.2	0.57	0.76	0.39	0.5
1995 Kobe	Takarazuka/000	6.9	1.2	0.69	0.69	0.50	1.1
1999 Chi-Chi Taiwan	CHY101/E	7.6	11.2	0.35	0.71	0.10	3.5
1999 Chi-Chi Taiwan	CHY128/N	7.6	9.7	0.17	0.69	0.09	4.5

by the senior authors [32] have shown that multidrum columns exhibit slightly more controlled response than the equal size monolithic configuration.

Our investigation proceeds by examining the response of the two abovementioned columns when subjected to the 11 historic records shown in Table II. The columns are considered to stand free on a rigid foundation, or standing free on a seismic isolated base with isolation periods $T_b = 2\,s$, 2.5 s and 3 s and linear viscous damping $\xi_b = 0.1$.

The dynamic analysis is conducted by assuming the idealized geometry of the columns. In reality some of these columns have suffered local chipping at the edges of the drums, while some drums may have experienced minor horizontal dislocations—a situation that not only may affect the planar rocking motion of the column, but also may accentuate the initiation of three-dimensional response, which is beyond the scope of this study.

Table III summarizes the results from the nonlinear time history analysis assuming planar motion. The column from the Temple of Apollo at Bassae ($R = 3.03\,m$, $\alpha = 10.56^\circ$) when standing free on a rigid foundation survives all the induced records, while when isolated on bearings that offer an isolation period, $T_b = 2.0\,s$, it topples in all but one records. As the period of the isolation system increases the column survives additional records. Similarly, the column for the Temple of Zeus a Nemea ($R = 5.22\,m$, $\alpha = 8.37^\circ$) when standing free on a rigid foundation survives 9 out of the 11 records, while when isolated on bearings that offer an isolation period $T_b = 2.0\,s$ it topples in all records.

Again, as the isolation period increases the column survives additional records; however, even when the isolation period is $T_b = 3.0\,s$ the column from the Temple of Zeus at Nemea survives only 3 out of the 11 records. The reason that seismic isolation is so detrimental to the stability of tall slender blocks is because the presence of the isolation system lengthens the duration of the pulses while at the same time increases the number of the significant induced cycles.

As an example, Figure 12 plots the response of a rigid block with the dimensions of a column of a column from the peristyle of the Temple of Zeus at Nemea subjected to the 022 component of the Jensen Filter Plant record from the 1994 Northridge earthquake when is standing free on a rigid foundation (left—no overturning) and when standing free on an isolated base with $T_b = 3.0\,s$ (right—overturning).

CONCLUSIONS

In this paper the seismic response analysis and stability of slender rigid blocks standing free on a seismically isolated base is investigated in depth. The paper examines the rocking response when the isolated base is supported: (a) on linear viscoelastic bearings, (b) on single concave and (c) on DCSS bearings. Our study revisits the equations of motion and settles the matter of the conservation of linear momentum of the entire moving system that is the

DOI: 10.1002/eqe

Table III. Stability results for the rigid blocks corresponding to the columns of the Temples of Bassae and Nemea when subjected to the 11 earthquakes. ($\surd$ = no overturn, $\times$ = overturn).

		Columns from the Temple of Apollo at Bassae ($R = 3.03$ m, $\alpha = 0.1844$)				Columns from the Temple of Zeus at Nemea ($R = 5.22$ m, $\alpha = 0.1461$)			
Earthquake	Record station	Non-isolated	$T_I = 2$s	$T_I = 2.5$s	$T_I = 3$s	Non-isolated	$T_I = 2$s	$T_I = 2.5$s	$T_I = 3$s
1966 Parkfield	CO2/065	$\surd$	$\times$	$\surd$	$\surd$	$\surd$	$\times$	$\times$	$\surd$
1977 Bucharest		$\surd$	$\times$	$\times$	$\surd$	$\surd$	$\times$	$\times$	$\times$
1979 Imperial Valley	El Centro #6/230	$\surd$	$\times$	$\times$	$\times$	$\surd$	$\times$	$\times$	$\times$
1980 Irpinia, Italy	Sturno/270	$\surd$	$\times$	$\times$	$\times$	$\surd$	$\times$	$\times$	$\times$
1986 San Salvador	Geotech Investig. Center	$\surd$	$\times$	$\surd$	$\surd$	$\surd$	$\times$	$\surd$	$\surd$
1987 Superstition Hills	Parachute Test Site/225	$\surd$	$\times$	$\times$	$\times$	$\times$	$\times$	$\times$	$\times$
1992 Erzican,	Erzincan/EW	$\surd$	$\times$	$\times$	$\surd$	$\times$	$\times$	$\times$	$\times$
1994 Northridge	Jensen Filter Plant/022	$\surd$	$\times$	$\times$	$\times$	$\surd$	$\times$	$\times$	$\times$
1995 Kobe	Takarazuka/000	$\surd$	$\times$	$\surd$	$\surd$	$\surd$	$\times$	$\times$	$\surd$
1999 Chi-Chi Taiwan	CHY101/E	$\surd$	$\surd$	$\times$	$\times$	$\surd$	$\times$	$\times$	$\times$
1999 Chi-Chi Taiwan	CHY128/N	$\surd$	$\times$	$\surd$	$\surd$	$\surd$	$\times$	$\times$	$\times$

DOI: 10.1002/eqe

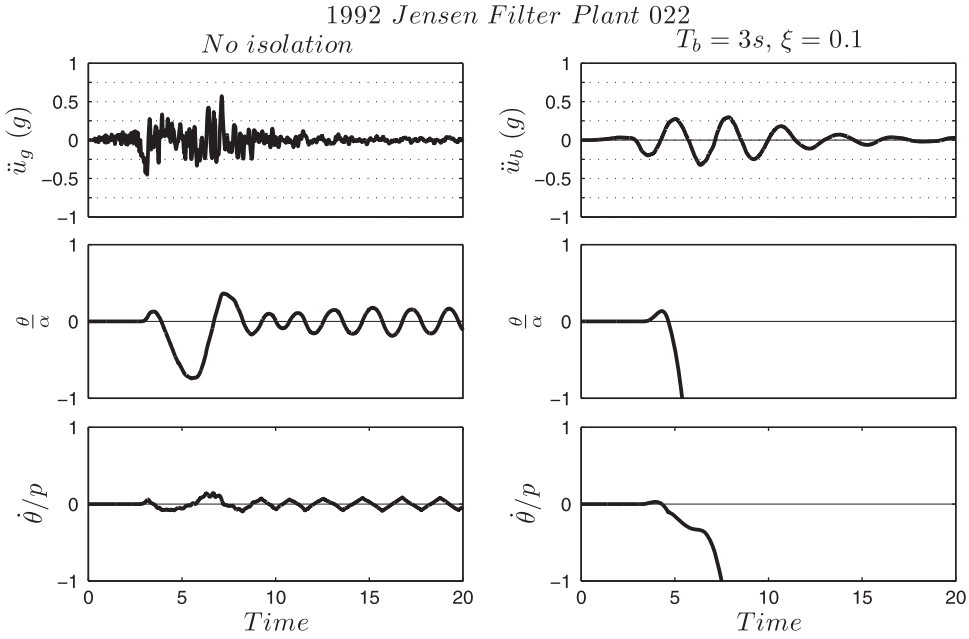

Figure 12. Comparison of the response of a rigid block with the dimensions of a column from the peristyle of the Temple of Zeus at Nemea subjected to the 022 component of the Jensen Filter Plant record from the 1994 Northridge earthquake when is standing free on a rigid foundation (left—no overturning) and when standing free on an isolated base with $T_b = 3.0$ s (right—overturning).

rocking—translating block together with the translating isolated base. This analysis leads to a closed-form expression (Equation (20)) for the maximum value of the coefficient of restitution during impact that allows rocking motion of a block rocking on an isolated base and is concluded that this value is always smaller (more energy is dissipated) than the maximum value, $r = (1 - \frac{3}{2}\sin^2\alpha)^2$ which is associated with a rigid block rocking on a rigid (non-isolated) foundation. Our extended parametric analysis concludes that seismic isolation is beneficial for relative small blocks. This happens because while seismic isolation increases the 'static' overturning acceleration; for isolated rigid blocks this 'static' value remains nearly constant as the ratio ω_p/p increases (moving to toward larger blocks or higher frequency pulses). Consequently, while the presence of an isolation base increases the 'static' overturning acceleration; it removes appreciably from the dynamics of rocking blocks the fundamental property of increasing stability as their size increases or the excitation pulse period decreases. This behavior prevails regardless whether the rocking block is supported on an isolated base with linear viscoelastic or spherical sliding bearings with single or double curvature. Nevertheless, the finding that seismic isolation increases the value of the ground acceleration that is needed to uplift a free-standing slender object is of major practical significance when protecting museum artifacts where any kind of damage due to impact shall be avoided.

The longer the isolation period of the supporting base is, the more stability is offered to the rocking blocks; however, large blocks subjected to moderate period pulses (say $\omega_p/p > 6$) exhibit superior stability when they stand free on a rigid base (non-isolated) rather when they are isolated even on isolation systems with very long periods. This remarkable result suggests that, given the seismicity of Greece, free-standing ancient classical columns when subjected to ground motions with moderate period predominant pulses so that $\omega_p/p < 6$ exhibit superior stability as they are built (standing free on a rigid foundation) rather than if they were seismic isolated. In conclusion, given that the rocking response of free-standing columns is a highly nonlinear problem, in association with the event that the edges of the columns may be damaged to an extend that the column departs appreciably from its idealized geometry further analysis may be required for deciding on the seismic protection/intervention of a specific monument.

DOI: 10.1002/eqe

ACKNOWLEDGEMENTS

Partial financial support for this study has been provided to the first author by the Alexander S. Onassis Public Benefit Foundation and by the EU research project 'DARE' ('Soil–Foundation–Structure Systems Beyond Conventional Seismic Failure Thresholds: Application to New or Existing Structures and Monuments'), which is funded through the 7th Framework Programme 'Ideas,' Support for Frontier Research—Advanced Grant, under contract number ERC-2—9-AdG 228254-DARE to Professor G. Gazetas.

REFERENCES

1. Housner GW. The behaviour of inverted pendulum structures during earthquakes. *Bulletin of the Seismological Society of America* 1963; **53**(2):404–417.
2. Augusti G, Ciampoli M, Airoldi L. Mitigation of seismic risk for museum contents. *Proceedings of the 10th World Conference in Earthquake Engineering*, Madrid, 1992; 5995–6000.
3. Vestroni F, Di Cinto S. Base isolation for seismic protection of statues. *Twelfth World Conference on Earthquake Engineering*, New Zealand, 2000.
4. Calio I, Marletta M. Passive control of the seismic response of art objects. *Engineering Structures* 2003; **25**:1009–1018.
5. Roussis PC, Pavlou EA, Pisiara EC. Base-isolation technology for earthquake protection of art objects. *The 14th World Conference on Earthquake Engineering*: *Innovation Practice Safety*, Beijing, China, October 2008.
6. Contento A, Di Egidio A. Investigations into benefits of base isolation for non-symmetric rigid blocks. *Earthquake Engineering and Structural Dynamics* 2009; **38**:849–866.
7. Yim CS, Chopra AK, Penzien J. Rocking response of rigid blocks to earthquakes. *Earthquake Engineering and Structural Dynamics* 1980; **8**(6):565–587.
8. Makris N, Roussos Y. Rocking response of rigid blocks under near-source ground motions. *Geotechnique* 2000; **50**(3):243–262.
9. Zhang J, Makris N. Rocking response of free-standing blocks under cycloidal pulses. *Journal of Engineering Mechanics*, *ASCE* 2001; **127**(5):473–483.
10. Veletsos AS, Newmark NM, Chelepati CV. Deformation spectra for elastic and elastoplastic systems subjected to ground shock and earthquake motions. *Proceedings of the 3rd World Conference on Earthquake Engineering*, vol. II. Wellington, New Zealand, 1965; 663–682.
11. Hall JF, Heaton TH, Halling MW, Wald DJ. Near-source ground motion and its effects on flexible buildings. *Earthquake Spectra* 1995; **11**(4):569–605.
12. Makris N. Rigidity–plasticity–viscosity: can electrorheological dampers protect base-isolated structures from near-source ground motions? *Earthquake Engineering and Structural Dynamics* 1997; **26**:571–591.
13. Makris N, Chang S-P. Effect of viscous, viscoplastic and friction damping on the response of seismic isolated structures. *Earthquake Engineering and Structural Dynamics* 2000; **29**(1):85–107.
14. Alavi B, Krawinkler H. Effects of near-source ground motions on frame-structures. *Technical Report No. 138*, The John A. Blume Earthquake Engineering Center, Stanford University, 2001.
15. Mavroeidis GP, Papageorgiou AS. A mathematical representation of near-fault ground motions. *Bulletin of the Seismological Society of America* 2003; **93**(3):1099–1131.
16. Ricker N. Further developments in the wavelet theory of seismogram structure. *Bulletin of the Seismological Society of America* 1943; **33**:197–228.
17. Ricker N. Wavelet functions and their polynomials. *Geophysics* 1944; **9**:314–323.
18. Addison P. *The Illustrated Wavelet Transform Handbook*: *Introductory Theory and Applications in Science*, *Engineering*, *Medicine and Finance*. Institute of Physics: London, U.K., 2002.
19. Apostolou M, Gazetas G, Grini E. Seismic response of slender rigid structures with foundation uplift. *Soil Dynamics and Earthquake Engineering* 2007; **27**:642–654.
20. Gazetas G, Garini E. Anastasopoulos I. Effect of near-fault ground shaking on sliding systems. *Journal of Geotechical Engineering* (ASCE) 2009; **135**(12):1906–1921.
21. Makris N, Black CJ. Dimensional analysis of rigid-plastic and elastoplastic structures under pulse-type excitations. *Journal of Engineering Mechanics* (ASCE) 2004; **130**(9):1006–1018.
22. Vassiliou MF, Makris N. Estimating time scales and length scales in pulse-like earthquake acceleration records with wavelet analysis. *Bulletin of the Seismological Society of America* 2011; **101**(2). DOI: 10.1785/0120090387.
23. MATLAB Version 2007b. *The Language of Technical Computing*. The Mathworks, Inc.: Natick, MA, 1999.
24. Makris N, Vassiliou MF. The existance of 'complete similarities' in the response of seismic isolated structures subjected to pulse like ground motions and their implications in analysis. *Earthquake Engineering and Structural Dynamics* (in print).
25. Makris N, Black CJ. Dimensional analysis of bilinear oscillators under pulse-type excitations. *Journal of Engineering Mechanics* (ASCE) 2004; **130**(9):1019–1031.
26. Hyakuda T, Saito K, Tanaka N, Yoneki S, Miyazaki M, Sawada T. The structural design and earthquake observation of a seismic isolated building using friction pendulum system. *The 7th International Seminar on Seismic Isolation*, *Passive Energy Dissipation and Active Control of Vibrations of Structures*, Assisi, Italy, 2–5/10, 2001.

27. Constantinou M. Friction Pendulum Double Concave Bearing. *Technical Report*. Available from: http://nees.buffalo.edu/docs/dec304/FP-DC%20Report-DEMO.pdf, 2004.
28. Tsai CS, Chiang TC, Chen BJ. Experimental evaluation piecewise exact solution for predicting seismic responses of spherical sliding type isolated structures. *Earthquake Engineering and Structural Dynamics* 2005; **34**(9): 1027–1046.
29. Fenz DM, Constantinou MC. Behavior of the double concave friction pendulum bearing. *Earthquake Engineering and Structural Dynamics* 2006; **35**(11):1403–1424.
30. Tsai CS, Chen WS, Chiang TC, Chen BJ. Component and shaking table tests for full-scale multiple Friction Pendulum system. *Earthquake Engineering and Structural Dynamics* 2006; **35**(11):1653–1675.
31. Psycharis IN, Papastamatiou DY, Alexandris AP. Parametric investigation of the stability of classical columns under harmonic and earthquake excitations. *Earthquake Engineering and Structural Dynamics* 2000; **29**(8):1093–1109.
32. Konstantinidis D, Makris N. Seismic response analysis of multidrum classical columns. *Earthquake Engineering and Structural Dynamics* 2005; **34**(10):1243–1270.

DOI: 10.1002/eqe